ADVANCED MATERIALS

Supporting Information

for *Adv. Mater.,* DOI: 10.1002/adma.202108788

Modularizable Liquid-Crystal-Based Open Surfaces Enable Programmable Chemical Transport and Feeding using Liquid Droplets

Yang Xu, Yun Chang, Yuxing Yao, Meng Zhang, Robert L. Dupont, Adil M. Rather, Xiaoping Bao, and Xiaoguang Wang**

WILEY-VCH

Supporting Information

Modularizable Liquid-Crystal-Based Open Surfaces Enable Programmable Chemical Transport and Feeding using Liquid Droplets

Yang Xu, Yun Chang, Yuxing Yao, Meng Zhang, Robert L. Dupont, Adil M. Rather, Xiaoping Bao, Xiaoguang Wang**

Materials and Methods

Materials

The following liquid crystals (LCs) were purchased from Jiangsu Hecheng Advanced Materials Co., Ltd: 1,4-bis-[4-(3-acryloyloxypropyloxy)benzoyloxy]-2-methylbenzene (RM257), 4'-pentyl-cyanobiphenyl (5CB), N-(4-methoxybenzylidine)-4'-butylaniline (MBBA) and E7. The chiral LC CB15 was purchased from Merck Co., Ltd. The water-soluble dyes (methyl orange and ethyl orange), anionic surfactant sodium dodecyl sulfate (SDS), nonionic surfactant Brij@C10 (average molecular weight is approximately 683 g/mol), dimethyloctadecyl [3-(trimethixysilyl) propyl]ammonium chloride (DMOAP; 42 wt% in methanol), photoinitiator 2,2-dimethoxy-2-phenylacetophenone (DMPAP), poly(pyromellitic dianhydride-*co*-4,4'-oxydianiline) amic acid, 1-methyl-2-pyrrolidinone, lithium phenyl-2,4,6-trimethylbenzoylphosphinate (LAP), acrylic acid (AA) and poly(ethylene glycol) methyl ether acrylate (PEGMEA; average number average molecular weight is 480 g/mol), PBS -/-, paraformaldehyde, CD31-APC, CD34-FITC, cardiac Troponin T (cTnT), 4',6'-Diamidino-2-phenylindole (DAPI) were purchased from Sigma-Aldrich. Magnesium chloride ($MgCl_2$), magnesium sulphate ($MgSO_4$), sodium chloride (NaCl), hydrogen chloride (HCl), sodium hydroxide (NaOH), iron (III) chloride ($FeCl_3$), sodium bicarbonate ($NaHCO_3$), silver nitrate ($AgNO_3$), potassium thiocyanate (KSCN), sodium carbonate (Na_2CO_3) and calcium chloride ($CaCl_2$) were purchased from Fischer Scientific. Human-induced pluripotent stem cells (hiPSCs), vascular endothelial growth factor (VEGF), Dulbecco's modified eagle medium (DMEM), ascorbic acid (Vc), CHIR99021 (CHIR), LaSR Basal medium, RPMI Basal medium, RPMI B27–, RPMI B27+, and Wnt-C59 were purchased from WiCell. Water used in all the experiments was purified using a Milli-Q water purification system (Simplicity C9210). Plain microscope slides (25 mm × 75 mm × 1 mm) and 2-well cell culture chamber slides were purchased from Fisher Scientific. The magnet was purchased from K&J Magnetics, Inc. Unless stated otherwise, purchased chemicals were used as received without further modification or purification.

Preparation of silane (DMOAP)-functionalized glass slides

First, glass slides were washed with water (10 mL) and ethanol (10 mL) and dried under a stream of nitrogen gas. Then, the clean glass slides were put in a 1% v/v DMOAP water solution (120 mL) for 15 min. After that, the glass slides were washed with water (10 mL) and ethanol (10 mL) to remove residual unreacted DMOAP molecules. Next, the silane-functionalized glass slides were dried under a stream of nitrogen gas. Finally, the obtained silane-functionalized

glass slides were stored in a dark place at ambient temperature and pressure to prevent light from damaging the silane coating.

Preparation of polyimide-coated glass slides

First, rinsed glass slides were spin-coated with a mixture of poly(pyromellitic dianhydride-*co*-4,4'-oxydianiline) amic acid (10% v/v) and 1-methyl-2-pyrrolidinone (90% v/v) at 4,000 rpm for 2 min by using a Laurell WS-650Mz-23NPPB spin processor. The glass slides were then heated at 350^{o}C for 3 h. Next, a velvet cloth was used to rub the formative polyimide coating on the glass slides unidirectionally 60 times. Finally, two rubbed polyimide glass slides were paired together (oriented to induce a 0^{o} twist) with 100 μm-thick spacers to fabricate optical cells.

Preparation of LC-based open surfaces

First, an LC mixture containing 10 wt% of a reactive LC monomer (RM257) and 90 wt% of a non-reactive LC mesogen (5CB) was prepared. DMPAP, a photoinitiator, was added to the LC mixture at 1 wt% based on the total mass of the LC mixture. Next, we uniformly spread 100 μL of the above homogenous LC mixture on a 25 mm × 25 mm × 1 mm silane (DMOAP)-functionalized glass slide. It was then placed under a UV lamp (Spectroline, EA-140; 365 nm) that provided 2.0 mW/cm^2 for 20 min at room temperature to prepare an approximately 160 μm-thick 5CB-swollen porous polyRM257 substrate. Finally, we drop-cast 80 μL of the same non-reactive LC mesogen (5CB) onto the 5CB-swollen polyRM257 porous structure to form a LC-based open surface. The optical appearance of the 5CB surface in the air was imaged using an Olympus BX53 microscope equipped with crossed polarizers. We used this method to prepare a LC coating on other substrates, including aluminum foil, tin, wood, steel, rubber, and cotton fabric.

Characterization of the morphology of porous polyRM257 substrates

The porous polyRM257 substrate used for the scanning electron microscopy (SEM) imaging was prepared from the photopolymerization of a mixture of 10 wt% RM257 in 5CB followed by an extraction of the nonreactive 5CB with ethanol (20 mL). After being fully dried, the porous substrate was coated with a thin layer of gold before imaging. Finally, the morphology of the porous polyRM257 substrate was imaged using an FEI Quanta 200 SEM with an acceleration voltage of 5 kV at a working distance of 9 mm.

Contact angle goniometer measurement

A KRÜSS DSA 100 goniometer was used to measure the contact angles and sliding angles of the water droplets on the LC surfaces using the sessile drop method. To determine the contact angle and sliding angle of water on these surfaces, 2 µL water droplets were deposited on the surface through a needle at a rate of 5 µL/min. For the sliding angle measurements, the LC surface was tilted at a rate of 1°/min and the angle at which the droplet began to move was taken as the sliding angle. During these measurements, a Linkam PE120 Peltier hot stage was used to control the temperature of the LC surfaces.

Stability and durability test of LC-based open surfaces

In the first set of experiments, we connected two individual LC surfaces together and made four independent scratches on the LC surfaces using a razor. We investigated the sliding behavior of water droplets on the LC platform by placing a 10 µL water droplet on the platform tilted at a 30º inclination. In the second set of experiments, we sought to investigate the effect of pH on the stability of the LC surfaces. We placed aqueous droplets with different pH values ranging from 1 to 13 using a concentrated HCl solution (6 M) and NaOH pellets and measured the sliding angles. Finally, we immersed the LC surfaces in water for 30 days to test the water durability of the LC surfaces by examining the sliding angle of the water droplet during this period.

Methods of loading chemicals into LC-based open surfaces

We used two different methods to load ethyl orange into the LC surfaces. *Co-solvent method:* We used ethanol as a co-solvent to prepare an ethyl orange/ethanol/LC mixture, where the concentration of ethyl orange was 0.4 wt% based on the mass of the LC. Subsequently, the ethanol was evaporated in a vacuum oven, resulting in the formation of nanometer-sized aggregates of ethyl orange within the LCs. Finally, we drop-cast the obtained mixture onto the surface of the porous polyRM257 to develop a chemical-loaded LC surface. *Aqueous droplet dispersion method*: We mixed an aqueous solution containing SDS at 5 mM and ethyl orange at 1 mM. This solution was then mixed at 20 wt% with an additional 80 wt% of a pure LC at 25°C to make ethyl orange aqueous microdroplets dispersed in the LC. Next, we drop-cast this dispersion onto the surface of the porous polyRM257 network. Finally, we used optical cells and polarized light microscopy to image the ordering of the nematic LC around the ethyl orange guest objects prepared by the two different methods (Figure S2, Supporting Information). The

thickness of the optical cells was 100 μm. The optical cells were prepared by pairing two rubbed, polyimide-coated glass slides.

Dynamic light scattering measurement of nanometer-sized dye aggregates

The hydrodynamic radius of the nanometer-sized ethyl orange aggregates (0.4 wt% based on the mass of the LC) prepared by the co-solvent method in the bulk LC was characterized with a Zeta-PALS analyzer (Brookhaven Instruments Corporation, Holtsville, NY). The LC containing the nanosized aggregates was further diluted by adding 33% v/v of dichloromethane (based on the total volume of LC) to induce an isotropic phase for dynamic light scattering (DLS) measurements. The number-average radii of ethyl orange nanoaggregates were calculated from at least six independent measurements.

Chemical loading and release determined by gravimetry

Chemical release from the LC surfaces was quantified using gravimetry. Specifically, we first measured the mass of the 5CB-swollen polyRM257 porous structures on a silane (DMOAP)-functionalized glass substrate (m_1) using a Mettler Toledo analytical balance. Next, we drop-cast chemical-loaded 5CB onto the 5CB-swollen polyRM257 porous structure and recorded its mass (m_2). The mass of the loaded chemicals was calculated as $(m_2 - m_1)\, y$, in which y is the mass fraction of the loaded chemicals based on the mass of the chemical-loaded 5CB. After the activated release of the chemicals to the water droplets placed on the 5CB surface, we removed the water droplets and measured the mass of the 5CB surface (m_3). The mass of the released chemicals was calculated as $m_2 - m_3$, and the percentage of the chemicals released from the 5CB surface was calculated as:

$$\text{Percentage of chemical release} = (m_2 - m_3) / [(m_2 - m_1)\, y] \times 100\% \quad \text{(S1)}$$

UV–visible spectrophotometry measurement

The concentration of the dyes in the water droplets was determined using a Perkin Elmer Lambda 950 UV–visible spectrophotometer. After releasing the chemicals into the water droplets that had been placed on the 5CB surface, we withdrew 3 μL aliquots from the droplet, placed them into UV cuvettes, and diluted them with 997 μL of water. Then, we measured the UV–visible absorption spectra ranging from 200 nm to 800 nm.

Immediate release of chemicals from LC-based open surfaces

We placed a 10 μL water droplet onto a 2.5 cm × 2.5 cm 5CB surface that was loaded with nanometer-sized ethyl orange aggregates using the co-solvent method described above. We observed that the droplet turned orange, indicating that the embedded ethyl orange molecules were continuously released into the aqueous droplet (see Movie S1). In addition, we added 5 mM SDS into the ethyl orange/ethanol/LC mixture to make nanometer-sized ethyl orange aggregates doped with SDS using the co-solvent method described above. After a 10 μL water droplet was placed on the surface (at 25°C, nematic phase), the encapsulated ethyl orange aqueous microdroplets immediately began to release and approximately 80% of them were found to have been released after 60 s, which is consistent with the result of Figure 2c in the main text. Therefore, the presence of SDS does not affect the immediate release of the ethyl orange aggregates from the LC surface.

Thermally triggered release of chemicals from LC-based open surfaces

For these experiments, all LC surfaces had dimensions of 2.5 cm × 2.5 cm and were loaded with aqueous microdroplets of ethyl orange using the aqueous droplet dispersion method described above. We placed a 10 μL water droplet on a nematic 5CB surface loaded with the aqueous microdroplets of ethyl orange at 25°C. Upon increasing the temperature to 40°C (nematic–isotropic phase transition temperature ($T_{N–I}$) for 5CB is 35°C), the release of the ethyl orange microdroplets into the water droplet was triggered (see Movie S1). We also used a 5CB/CB15 (80 wt%/20 wt%) mixture, 5CB/RM257 (60 wt%/40 wt%) mixture, and E7 in place of the pure 5CB on the LC-based open surfaces, showing the $T_{N–I,}$ and thus the threshold temperature for chemical release at the LC surface can be tuned over a wide temperature range (e.g., from 10°C to 92°C). To study the effect of inorganic and organic chemicals and surfactants on the release of microdroplets from the LC surface, we added guest objects, including inorganic particles such as 1 mg of $CaCO_3$ or Fe_3O_4, organic molecules such as glycerol (2 mM), or surfactants such as SDS (5 mM), into a 10 μL aqueous droplet which was then put on the ethyl orange aqueous microdroplet-loaded LC surface. We found that these guest materials in the droplet on the surface do not affect the release of the microdroplets from the LC surface after a heat-induced nematic to isotropic phase transition of 5CB.

Sequential reactions within water droplets on LC-based open surfaces

In this set of experiments, we prepared a 0.5 mM aqueous SDS solution consisting of 0.6 mM HCl and a 0.5 mM SDS solution consisting of 1 mM NaOH. These two solutions were then dispersed (80 wt%) in 5CB separately to load acidic and alkaline chemicals into the 5CB. We

then drop-cast 80 μL of the obtained chemical-loaded LC mixtures onto a 5CB-swollen porous polyRM257 substrate to prepare an "HCl" LC module and an "NaOH" LC module, respectively. Next, we integrated the LC surfaces in the sequence of initial–HCl–NaOH, where the "initial" module refers to a pure LC surface. We placed a 10 μL orange droplet of aqueous methyl orange (0.5 mM) onto the surface of the initial module at 25°C and moved the droplet from the initial module to the HCl module. The temperature of the HCL module was increased to 40°C (isotropic) to release the loaded HCl into the droplet, resulting in an orange-to-red color transition of the droplet on the surface. After 40 s, the HCl module was cooled down to 25°C and the droplet on the surface was moved to the NaOH module. The droplet was initially red but turned yellow after the temperature of the NaOH module increased to 40°C (see Movie S1). The same experimental procedure was used for the sequence of initial–NaOH–HCl with no observed orange-to-red color change (see Figure 3 in the main text).

Parallel reaction within water droplets on LC-based open surfaces

In this set of experiments, we prepared three individual 0.5 mM aqueous SDS solutions containing 1 mM $AgNO_3$, 1 mM KSCN, and 1 mM $NaHCO_3$, respectively. Next, the three aqueous solutions were separately dispersed in 5CB (80 wt%), and 80 μL of each was coated separately on three 5CB-swollen porous polyRM257 substrates to prepare LC surfaces loaded with different chemicals, namely $AgNO_3$, KSCN, and $NaHCO_3$. We integrated the LC surfaces in the sequential order of initial–$AgNO_3$–KSCN–$NaHCO_3$. Next, we placed three aqueous droplets of 0.5 mM $FeCl_3$ on the initial LC surface, and selectively moved one $FeCl_3$ aqueous droplet to each LC module at 25°C. At this temperature, no chemical reaction was observed within all aqueous droplets. After heating the temperature of the LC surfaces above $T_{N–I}$ (40°C), the surfaces were activated, triggering the release of the chemicals into the $FeCl_3$ aqueous droplets, which caused the formation of a white precipitate in one droplet (AgCl), a red coloration of the second droplet ($Fe(SCN)_3$), and the formation of carbon dioxide (CO_2) bubbles in the last, with respect to the three LC surfaces.

Growth of calcium carbonate crystals in water droplets on LC-based open surfaces

We dispersed a 0.5 mM aqueous SDS solution consisting of 5 mM Na_2CO_3 with 5CB (80 wt%). Next, we drop-cast 80 μL of the obtained mixture onto a 5CB-swollen polyRM257 porous substrate to prepare the Na_2CO_3 module. Then we placed a 10 μL aqueous droplet consisting of 0.1 mM $CaCl_2$ on the Na_2CO_3-loaded LC module. After triggering the release of Na_2CO_3 by heating the LC surface to 40°C, we observed a formation of white $CaCO_3$ crystals within the

aqueous droplet. Finally, we collected the formed crystals for further characterization. We note here that the aqueous droplets containing $CaCO_3$ crystals can freely slide on the LC surface without severe pinning, revealing an excellent liquid repellency and slipperiness.

X-ray diffraction analysis of calcium carbonate crystals

X-ray diffraction (XRD) analysis of the $CaCO_3$ crystals was carried out by means of a Panalytical X'pert Pro PW 3040/60 powder diffractometer using Cu Kα radiation and operating at 40 mA and 45 kV. The 2θ range was from 20° to 70° at a scan rate of 0.03° per step.

(Co)polymerization in water droplets on LC-based open surfaces

We prepared three separate aqueous SDS solutions (0.5 mM) consisting of 1 mM AA, 1 mM PEGMEA, and 0.1 mM LAP, a photoinitiator, and separately dispersed the formed aqueous solutions into 5CB (80 wt%). The respective LC surface modules were called AA, PEGMEA, and initiator. Next, we integrated the LC surfaces in the sequence of initial–AA–PEGMEA–initiator–final. To achieve a remote control over the motion of the water droplets on the LC surfaces, we added 0.1 mg of magnetic Fe_3O_4 particles into the water droplets and used an external magnetic field (0.56 T) to move them. We note here that the LC surfaces were cooled to the nematic phase when the water droplet was being moved from one LC module to another. The photopolymerization was performed on the final LC surface module. The composition of the obtained polymers (e.g., the content of AA or PEGMEA) can be tuned by the selective release of the respective monomers to the water droplets on the LC surfaces.

Characterization of polymers formed within water droplets on LC-based open surfaces

We used proton nuclear magnetic resonance spectroscopy (^{1}H NMR) to measure the composition of the polymers formed within the water droplets on the LC surfaces. The formed homopolymers and copolymers were dissolved in deuterium oxide and measured using a 400 MHz Avance NEO ^{1}H NMR, equipped with an autosampler. Gel permeation chromatography (GPC) was performed with two tandem I-series Mixed Bed Low MW ViscoGel columns (Viscotek) driven by an equipped Agilent 1260 series pump. A Wyatt DAWN EOS light scattering detector and an Optilab DSP differential refractive index detector were used to analyze the molecular weight and distribution of the obtained homopolymers and copolymers. Water was used as the mobile phase with a flow rate of 1 mL/min. Molecular weights and distributions were calculated based on the elution time of standard polyethylene glycol (PEG). In addition, the glass transition temperatures of the synthesized polymers were measured using

a TA differential scanning calorimeter (DSC) Q100 Instrument. The heating/cooling rate in the DSC measurement was 2°C/min.

Cytotoxicity analysis of LC

Cell viability was determined by MTS (Owen's reagent) assay. hiPSCs (1×10^4) in 100 μL of culture medium were plated in each well of a 96-multiwell plate for overnight growth. The culture medium was removed, and hiPSCs were treated for 24 h with 100 μL of different ratios of LC, either MBBA or 5CB, to water ([LC]:[water] = 1:320, 1:640, 1:1,280, and 1:2,560). After treatment, the medium was removed, and the plates were washed three times with PBS. Each well received 100 μL of culture medium containing 16.7 vol% of MTS stock solution and was incubated for 1 h at 37°C in a humidified 5% CO_2 incubator. The plate was centrifuged at 2,000 gravitational acceleration for 10 min to spin down the cell debris, followed by a transfer of 80 μL of the supernatant into a new 96-well plate. The absorbance of formazan was analyzed at 490 nm on a Molecular Devices SpectraMax iD3.

Directed differentiation of hiPSCs using LC surfaces

19-9-11 hiPSCs were maintained on Matrigel-coated six-well plates in an mTeSR plus medium at 37°C in a humidified incubator in air with 5% CO_2. To differentiate hiPSCs into endothelial progenitors, hiPSCs were singularized with Accutase, then seeded onto the Matrigel-coated cell chamber in an mTeSR plus medium supplemented with 5 μM ROCK inhibitor Y-27632 for 24 h. On day 0, the culture medium was changed to a DMEM medium supplemented with 100 μg/mL ascorbic acid (DMEM/Vc) and the cells were treated with a 30 μL water droplet, which was kept on an isotropic MBBA LC surface that was loaded with a 20 vol% mixture of a 0.5 mM Brij@C10 aqueous solution containing a 60 μM aqueous solution of CHIR for 1 min. On day 1, the culture medium was changed to a LaSR basal medium.[1] From Day 2 to Day 5, the cell culture medium was changed daily with fresh LaSR basal medium, and the cells were treated with 30 μL water droplets, which had been kept on isotropic LC surfaces that had been loaded with 20 vol% mixtures of a 0.5 mM Brij@C10 aqueous solution containing 500 ng/mL VEGF for 1 min. On day 5, differentiated cells were collected for flow cytometry and immunostaining analysis. Local Joule heating was used to induce a phase change in these surfaces on demand. We also note here that every water droplet was infused with 0.1 mg of Fe_3O_4 magnetic particles. After chemical feeding from the isotropic LC surfaces, the droplet can be moved using an electromagnet into the hiPSC-containing culture medium. Using these

methods, the moving and chemical feeding of the droplet can be easily automated, which shows the potential utility of these LC-based surfaces.

To initiate cardiac differentiation of hiPSCs, the stem cell culture medium was changed to an RPMI basal medium on day 0 and the hiPSCs were treated with a 30 µL water droplet that had been kept on an isotropic LC surface that was loaded with a 20 vol% mixture of a 0.5 mM Brij@C10 aqueous solution containing 60 µM of CHIR for 1 min, followed by a medium change with RPMI basal medium supplemented with B27 without insulin (RPMI B27–) after 24 h. On day 3, the RPMI B27– culture medium was refreshed, and the differentiated cells were treated with a 30 µL water droplet that had been kept on an isotropic LC surface that was loaded with a 10 vol% mixture of a 20 µM aqueous solution of Wnt-C59 for 1 min. On day 5, the culture medium was refreshed. Starting from day 7, the culture medium was replaced with RPMI B27+ every 3 days until day 15 for sample collection and analysis. We note here that the nematic to isotropic phase transition of the MBBA LC surfaces was triggered by filling the chamber under the LC surface with 50^{o}C water and all the procedures were performed in a sterile biosafety cabinet.

Immunostaining analysis

Differentiated hiPSC cell cultures were washed with room temperature PBS-/- and fixed in a 4% paraformaldehyde PBS-/- solution for 15 min. Cells were then washed twice with PBS-/- and stained with CD31-APC and CD34-FITC for the differentiated endothelial progenitors or Cardiac Troponin T (cTnT) for the differentiated cardiac cells. 4',6'-Diamidino-2-phenylindole (DAPI) was used to stain the cell nuclei. A Leica DMi-8 fluorescent microscope was used for cell imaging.

Flow cytometry analysis

Cells were singularized with Accutase for 10 min at 37°C and pelleted by centrifuging for 5 min. Endothelial progenitor cells were washed once with FlowBuffer1 (PBS-/- solution supplemented with 0.5% BSA (w/v)) and then stained with CD31-APC and CD34-FITC in the dark for 25 min at room temperature. Cardiomyocytes were fixed in a 1% paraformaldehyde PBS-/- solution for 20 min, followed by permeabilization in cold 90% methanol for 1 h or overnight at –20°C. Permeabilized cells were washed twice with FlowBuffer2 (PBS-/- solution supplemented with 0.5% BSA (w/v) and 0.1% Triton X-100 (v/v)) and stained with a cTnT primary antibody, followed by a secondary antibody for 1 h at room temperature or 4°C

overnight. Stained cells were filtered through a 75 μm strainer and analyzed in a BD Accuri C6 plus flow cytometer.

Results

Stability criteria of LC-based open surfaces against dewetting by water droplets

Past studies have reported a water-induced dewetting of LC films coated on substrates that have been modified to be hydrophobic.[2] In this research, a porous polymeric substrate was created that can stabilize the LC films against water-induced dewetting. This section seeks to provide a theoretical investigation of the stability of the LC-based open surfaces against water-induced dewetting. Past studies have reported that porous substrates require a specific level of energy in order to stabilize a slippery, isotropic lubricant film against water-induced dewetting.[3] Aligned with this, we reason that the total interfacial energy of the water-wetted porous polyRM257 substrate (E_A) must be higher than that wetted by the LC with (E_1) or without (E_2) a water droplet on the surface. This can be written as:

$$\Delta E_1 = E_A - E_1 = r\,(\gamma_{LC}\cos\theta_{LC} - \gamma_w\cos\theta_w) - \gamma_{w\text{–}LC} > 0 \quad \text{(S2)}$$

$$\Delta E_2 = E_A - E_2 = r\,(\gamma_{LC}\cos\theta_{LC} - \gamma_w\cos\theta_w) + \gamma_w - \gamma_{LC} > 0 \quad \text{(S3)}$$

in which r is the roughness factor (or the ratio of the true versus the projected surface areas of the porous surface), $\gamma_{w\text{–}LC}$ is the interfacial tension between water and the LC film, γ_w and γ_{LC} represent the surface tension of water and the LC, respectively, and θ_w and θ_{LC} are the equilibrium contact angles between the water or the LC on a solid surface, respectively. The equilibrium contact angles and surface tensions of the water and 5CB on the polyRM257 surface were measured, as summarized in Table S1. Using the values from Table S1 and substituting them into Equations S2 and S3, the interfacial energies were calculated to be ΔE_1 = + 10.7 mJ/m^2 and ΔE_2 = + 68.4 mJ/m^2. These values remained positive even when r = 1, corresponding to flat surfaces. For reference, our porous polyRM257 surfaces have r > 1. These results imply that the LC film will be stable on the porous polyRM257 substrate through surface tension-induced capillary forces and will resist water-induced dewetting. This result makes them suitable as an open surface platform for droplet reactors.

Optical appearance of LC-based open surfaces under water droplets

The optical appearance of the LC-based open surfaces under water droplets was measured under a polarized light microscope. As shown in Figure S1 (Supporting Information), the nematic 5CB film adopts a dark appearance in the air and a bright appearance when in contact with a 2 µL water droplet. This transition is consistent with the different surface anchorings of nematic 5CB at the air–LC interface (perpendicular to the interface) and water–LC interface (parallel to the interface).[4] The conoscopic image further confirmed the homeotropic alignment of the

5CB at the interface between air and the 5CB surface and the interface between the 5CB and the polyRM257-coated substrate, as shown in the inset of Figure S1 (Supporting Information).

Generalizability of LC-based open surfaces for different substrates and their physical and chemical stability

In this section, we investigated the generizability and stability of our LC-based open surfaces. First, we fabricated LC surfaces on a variety of substrates, including aluminum foil, tin, wood, steel, rubber, and cotton fabric. As shown in Figure S14 (Supporting Information), water droplets exhibited a pinning-free sliding on inclined nematic LC surfaces coated on all of the substrates. Second, inspection of Figure S10 (Supporting Information) reveals that the LC surfaces remained slippery to water droplets after physical damage, and the water droplet could even cross the joint between two connected surfaces without severe pinning. Additionally, we tested the stability of our LC surfaces to water droplets with various pH values. As shown in Figure S11 (Supporting Information), water droplets with a wide range of pH values (e.g., 1–13) can slide without severe pinning on the inclined nematic LC surfaces. Finally, as can be seen in Figure S13 (Supporting Information), water droplets can still slide off of the nematic 5CB surface even after having been immersed in water for 30 days. These results demonstrate the generalizibility of our LC-based open surfaces to a wide range of substrates along with their resilience to a range of environments, including various pH levels and prolonged aqueous conditions.

Thermodynamic model for the release of chemicals from LC-based open surfaces

Our experimental observations in Figure 2b of the main text suggest that a nematic to isotropic phase transition can activate the release of chemical microdroplets (an aqueous solution of SDS and ethyl orange) into water droplets on the LC surfaces, while nanometer-sized chemical objects (ethyl orange aggregate) will immediately release regardless of the phase of the LC surface. Here we sought to derive a simple thermodynamic model to describe the key features of these different release behaviors. We will describe each interaction involved in the process of the activated release of the chemicals, mainly including the van der Waals forces and LC elastic forces. These two forces are combined into a thermodynamic model to describe the behaviors of droplets interacting with LC surfaces during the process of activated chemical release.

First, the attractive van der Waals forces (F_{vdW}) between the chemical microdroplets and the water droplet can be written as:[5]

$$F_{\mathrm{vdW}} = -\frac{A_{\mathrm{H}} R R_{\mathrm{chemical}}}{6x^2 (R_{\mathrm{chemical}}+R)} \quad \text{(S4)}$$

where A_{H} is the Hamaker constant for the interaction between air and water across a LC film, R_{chemical} is the radius of the chemical microdroplet, R is the radius of the water droplet on the LC surfaces, and x is the surface-to-surface distance between the chemical microdroplet and the water droplet. In our calculations, we assumed R_{chemical} = 5 μm and R = 1.34 mm. For R_{chemical} << R, Equation S4 can be simplified to:

$$F_{\mathrm{vdW}} = -\frac{A_{\mathrm{H}} R_{\mathrm{chemical}}}{6x^2} \quad \text{(S5)}$$

We note here that the negative sign in Equation S5 indicates that F_{vdW} is attractive in the process of chemical release (A_{H} (typical value is approximately 10^{-20} J)[5-6] is always positive).

Second, past studies have demonstrated that a repulsive interaction in bulk LC systems, caused by the long-range orientational ordering of the LCs, arises when the dispersed colloidal particles move towards a surface.[7] The LC elastic force (F_{elastic}) between the chemical microdroplet and water droplet interface can be calculated as:[7b]

$$F_{\mathrm{elastic}} = +\frac{\alpha^2 \beta \pi K R_{\mathrm{chemical}}^4}{(R_{\mathrm{chemical}}+x)^4} \quad \text{(S6)}$$

where α and β denote dipole and quadrupole moments carried by the chemical microdroplets in the LC and K denotes the Frank elastic constant of the LC. α is 2.04 for the chemical microdroplet while the LC has a homeotropic anchoring in the nematic phase when $R_{\mathrm{chemical}} > K/W$, and 0 for a chemical microdroplet when the LC is either in the isotropic phase or when $R_{\mathrm{chemical}} < K/W$ in the nematic phase.[7b, 8] β = 0.5 for homeotropic anchoring.[9] K is set to 5 pN.[4] The maximum F_{elastic} is +32.7 pN, calculated by Equation S6 with x = 0. We note here that the positive sign in Equation S6 indicates that the LC elastic force is always repulsive and hinders the release of chemical microdroplets.

Finally, we combined the above forces into a single model to describe the key features of the activated release behavior on LC-based open surfaces. From Equations S5 and S6, the net force (F_{net}) acting on the chemical microdroplet can be written as:

$$F_{\mathrm{net}} = F_{\mathrm{vdW}} + F_{\mathrm{elastic}} = -\frac{A_{\mathrm{H}} R_{\mathrm{chemical}}}{6x^2} + \frac{\alpha^2 \beta \pi K R_{\mathrm{chemical}}^4}{(R_{\mathrm{chemical}}+x)^4} \quad \text{(S7)}$$

We used Equation S7 to calculate F_{net} for the chemical microdroplets encapsulated in a nematic LC surface upon which a droplet of pure water has been placed. Figure S4 (Supporting Information) shows this net force, plotted alongside the individual forces from Equation S7. The repulsive F_{elastic} leads to a kinetic barrier (approximately 25 pN) that prevents the ejection of the chemical microdroplets, which is consistent with our experimental observation that no release of chemical microdroplets occurred from a nematic LC surface.

Then, we used Equation S7 to calculate F_{net} for the chemical microdroplets (5 mM SDS aqueous solution of ethyl orange) encapsulated in an isotropic LC surface with a droplet of pure water deposited on the surface. $F_{elastic} = 0$ when the LC is in the isotropic phase. As shown in Figure S4 (Supporting Information), the absence of the repulsive $F_{elastic}$ allows F_{net} to become negative (attractive) releasing the chemical microdroplets into the water droplet. This result confirms that the nematic to isotropic phase transition induced by heat can activate the release of chemical microdroplets from the isotropic LC surface, which leads us to conclude that the orientational order in the LCs play an essential role in chemical microdroplet release processes. Furthermore, when $R_{chemical} < K/W$ in the nematic phase, $F_{elastic} = 0$ and the consequent F_{net} becomes negative (attractive), supporting our observation that the nanometer-sized chemical aggregates will immediately release into the water droplet on the surface due to F_{vdW}, which is always negative.

Effect of Brownian motion and droplet movement on the transfer of microdroplets between different LC film modules

We first estimated the thermally-induced diffusion of aqueous microdroplets encapsulated in the LC film. The two-dimensional random diffusion of the microdroplets can be calculated as:

$$<x^2> = 4Dt = \frac{2k_B T}{3\pi\eta a} \quad \text{(S8)}$$

where $<x^2>$ is the mean square displacement, D is the diffusion coefficient, t is time, η is the viscosity of the LC (10^{-2} Pa s), and a is the hydrodynamic radius of the microdroplets in the LC. The time required for lateral diffusion of a 10 μm-in-diameter microdroplet over a distance of 1 mm within the LC film is estimated to be $> 3 \times 10^4$ hours. This calculation suggests that Brownian diffusion will not lead to a measurable transfer of microdroplets across different LC modules.

Second, we estimated the transfer of cargo carried by a moving water droplet on the surface of a LC film. The mass of the ethyl orange aqueous microdroplets in the LC film (2.5 cm × 2.5 cm) was approximately 12 mg. According to our previous study, we estimated the mass of the LC wetting ridge and wrapping layer around a 10 μL water droplet to be approximately 0.16 mg.[10] With such a small LC wetting ridge and wrapping layer, it is unable to transfer a large amount of cargo and is unable to cause a measurable change to the bulk properties of the other LC surfaces that the water droplet comes in contact with. To validate our analysis, we performed an additional experiment to determine whether or not droplet movement can induce the transfer of encapsulated microdroplets between LC film modules. Specifically, we first assembled an ethyl orange aqueous microdroplet-loaded LC module and a pure LC module together. Then

we added a 10 μL water droplet on the ethyl orange aqueous microdroplet-loaded LC module and tilted the surface to transport the droplet to the pure LC module. After evaporating the droplet, we took 5 μL of the LC that was near to and under the droplet position and diluted it with 1 mL ethanol to do UV-visible spectra tests, as shown in Figure S17 (Supporting Information). Our results demonstrate that the movement of a water droplet causes no measurable transfer of the encapsulated aqueous microdroplets between LC film modules.

XRD analysis of calcium carbonate crystals

XRD shows the characteristic peaks of calcite and vaterite in the formed crystals, as shown in Figure S7a (Supporting Information). The characteristic peaks at 2θ of 23.1°, 29.4°, 35.9°, 39.5°, 43.1°, 47.5° and 48.5° correspond to the (012), (104), (110), (113), (016), (018) and (116) crystallographic planes of calcite, and the peaks at 2θ of 24.92°, 26.99°, 32.78° and 43.8° correspond to the (100), (112), (114) and (300) lattice planes of vaterite.[11] These measurements reveal that a mixed crystallographic form was obtained on the LC surfaces. Additionally, we demonstrated that the crystal nucleation and growth can be performed for more than 100 successive cycles, as shown in Figure S7b (Supporting Information).

Cell viability and cytotoxicity analysis of LC

hiPSCs (1×10^4) in 100 μL of a culture medium were plated in each well of a 96-multiwell plate for overnight growth. After removal from the culture medium, the hiPSCs were treated with different ratios of LC to culture medium for 24 h. As shown in Figure S18 (Supporting Information), MBBA exhibits a lower cytotoxicity (cell viability >95%) in all tested ratios of MBBA to water ([MBBA]:[water] = 1:320, 1:640, 1:1,280, and 1:2,560), compared with 5CB (cell viability around 83% in the related mixture [5CB]:[water] = 1:320).

Table S1. Interfacial tension and contact angle measurements of water and LCs on porous substrates. $n = 3$ for the means and standard deviations.

θ_w (°)	86.5 ± 1.3
θ_{LC} (°)	0
γ_w (mN/m)	72.8 ± 1.4
$\gamma_{w–LC}$ (mN/m)	20.5 ± 1.3
γ_{LC} (mN/m)	35.6 ± 1.4

Table S2. Molecular weights of polymers synthesized within the water droplet reactors on LC surfaces.

Polymer	Number-average molecular weight (M_n; g/mol)	Weight-average molecular weight (M_w; g/mol)	Polydispersity index (M_w/M_n)
poly(AA-*co*-PEGMEA)	349,000	493,000	1.41
poly(PEGMEA)	279,000	336,000	1.20
polyAA	143,000	218,000	1.54

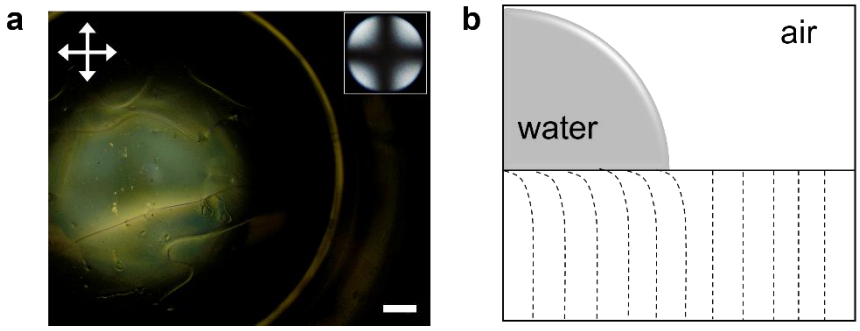

Figure S1. Orientational ordering of LCs within a nematic 5CB film underneath water droplets. Polarized light micrograph (top view) (a) and schematic illustration (side view) (b) of LC ordering within a nematic 5CB film underneath a 2 µL water droplet. Scale bar, 500 µm. Inset in (a) is a conoscopic image confirming the homeotropic alignment of the 5CB at the interface between air and the 5CB surface and the interface between the 5CB and a polyRM257-coated substrate. Crossed double-headed arrows in (a) indicate the orientation of the crossed polarizers and the black dashed lines in (b) indicate the local LC director. As can be seen in (a), the LC film remained between the water droplet and the polyRM257 porous substrate and was not de-wetted by the water droplet.

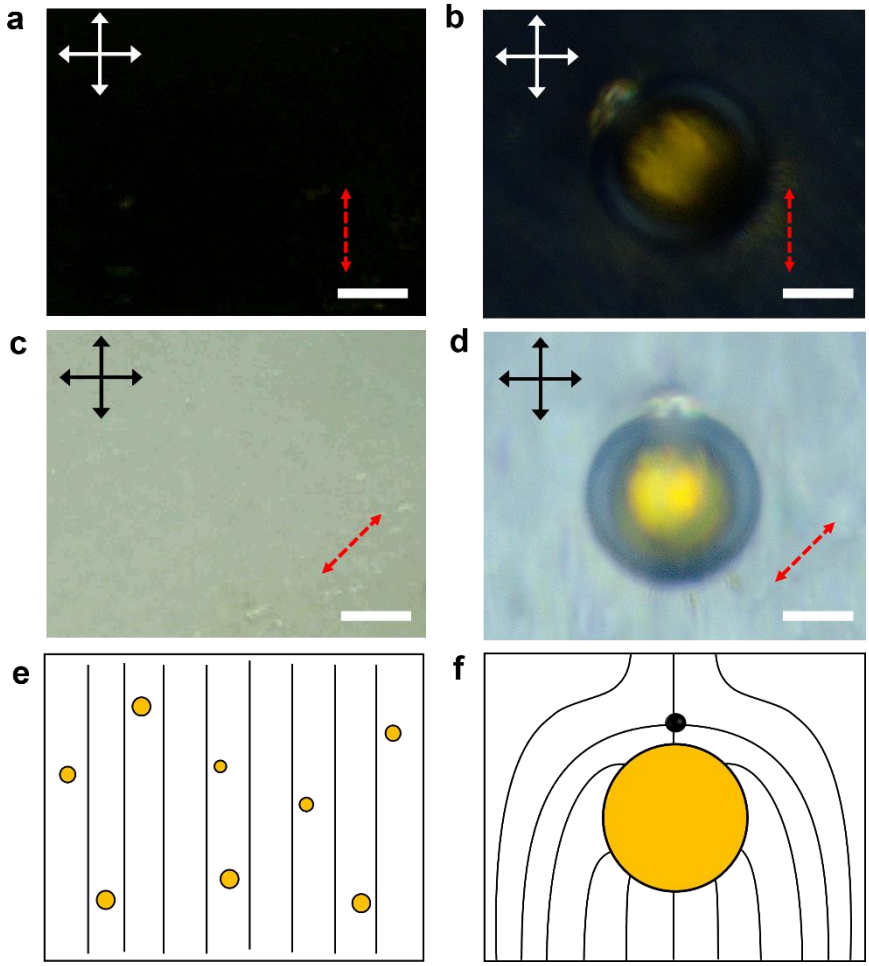

Figure S2. Size-dependent LC ordering around objects in bulk LC. Polarized light microscope images (a,b,c,d) and corresponding schematic illustrations (e,f) showing (a,c,e) nanometer-sized ethyl orange aggregates and (b,d,f) aqueous microdroplets of SDS and ethyl orange in bulk 5CB. Crossed double-headed arrows in (a,b,c,d) indicate the orientations of crossed polarizers. Red, double-headed dashed arrows in (a,b,c,d) indicate the rubbing direction. The black lines in (e,f) indicate the local LC director. Scale bars, 5 μm.

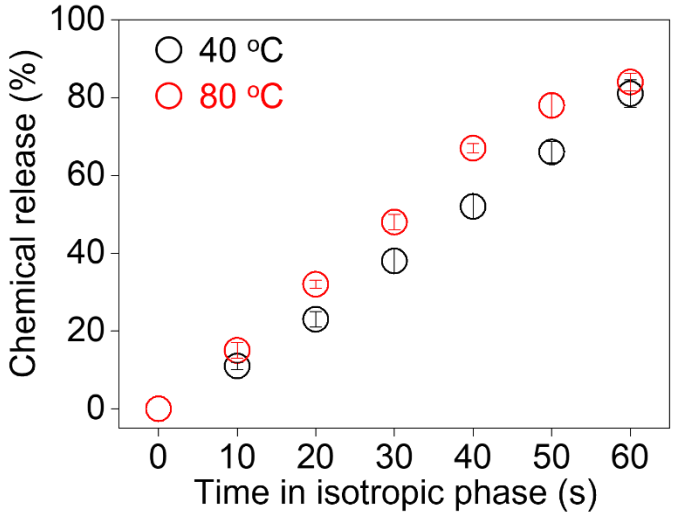

Figure S3. Plot showing the effect of the temperature of the LC film while in the isotropic phase (black, 40°C; red, 80°C) on the kinetics of the release of the ethyl orange aqueous microdroplets into the water droplet on the LC surface. The mass of the ethyl orange aqueous microdroplets in the LC film (2.5 cm × 2.5 cm) was approximately 12 mg.

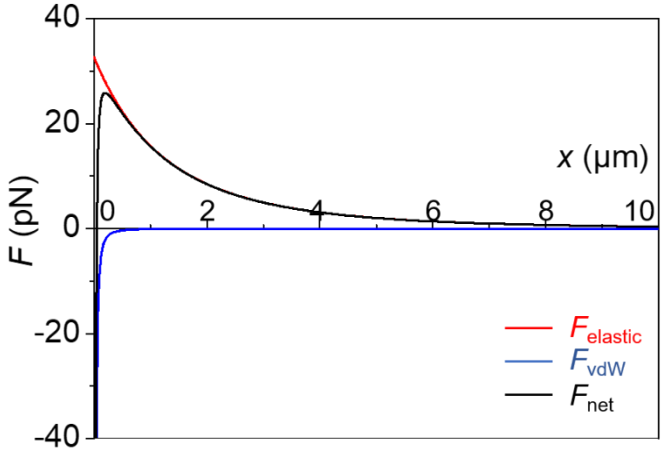

Figure S4. Calculated forces acting on chemical microdroplets in bulk LC. Forces [calculated using Equation (S7)] acting on chemical microdroplets as a function of the surface-to-surface distance between the chemical microdroplet and a water droplet on the surface (x). The radii of chemical aqueous microdroplets in the bulk LC and water droplets on the LC surface are 5 μm and 1.34 mm, respectively.

a

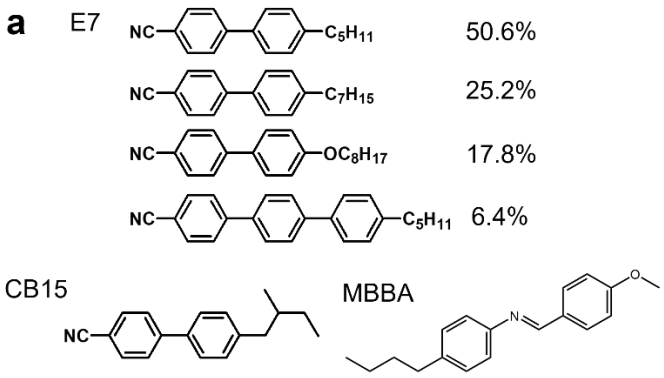

b

Liquid crystal composition (wt%)	Threshold $T_{N\text{-}I}$ (°C)
5CB/CB15 (80%/20%)	10
5CB	35
MBBA	47
E7	62
5CB/RM257 (60%/40%)	92

Figure S5. LCs with different nematic to isotropic phase transition temperatures. a) Chemical structures of E7, CB15, and MBBA. b) Phase transition temperatures of different LCs and LC mixtures.

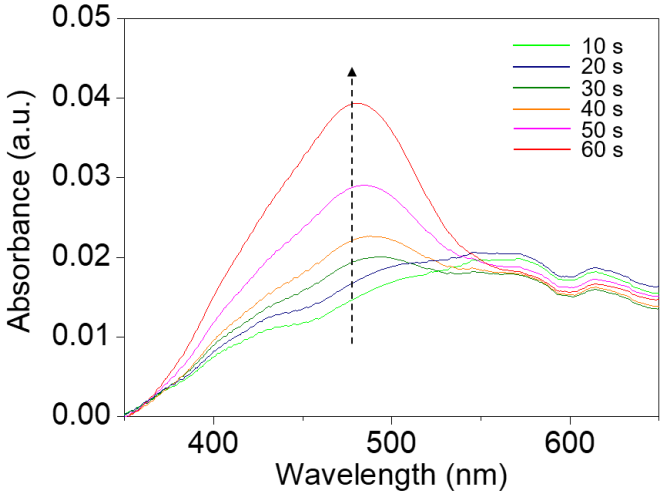

Figure S6. Effect of time spent in the isotropic phase on the dye release into water droplets on the LC-based open surface. UV–visible spectra of ethyl orange in water droplets on LC surfaces with different duration in the isotropic phase (40°C). The volume of the water droplets was 20 μL.

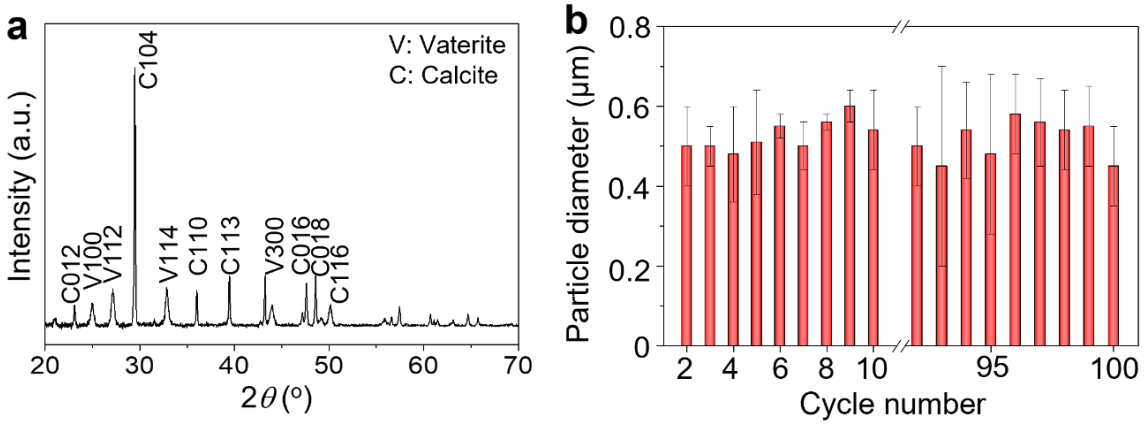

Figure S7. Synthesis of $CaCO_3$ crystals on LC surfaces. a) XRD spectrum of $CaCO_3$ crystals synthesized on the LC-based open surfaces. b) Plot showing the reusability of the LC-based open surfaces for $CaCO_3$ crystal nucleation and growth. Each cycle represents a 20 s period where the Na_2CO_3-loaded LC surface was in the isotropic phase with a water droplet on the surface. The volume of the $CaCl_2$ aqueous droplet was 10 μL, and the concentration of $CaCl_2$ was 0.1 mM. The LC surfaces encapsulated 12.5 vol% of a 5 mM aqueous solution of Na_2CO_3.

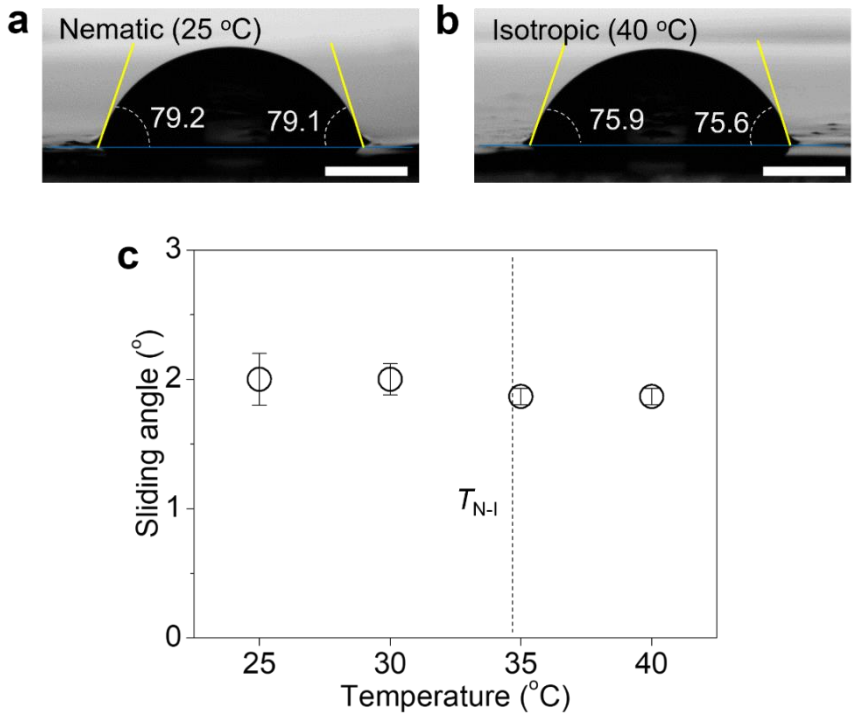

Figure S8. Apparent advancing contact angle and sliding angle of water droplets on LC-based open surfaces with and without loaded chemicals. a,b) The contact angle of water droplets on a nematic (25°C) (a) and isotropic (40°C) (b) 5CB surface without loaded chemicals. The droplet volume was 2 µL. Scale bars, 500 µm. c) Sliding angle of a 2 µL water droplet on a 5CB surface as a function of temperature. The vertical dashed line indicates the nematic to isotropic phase transition of 5CB. The mass of the ethyl orange aqueous microdroplets in the LC film (2.5 cm × 2.5 cm) was approximately 12 mg.

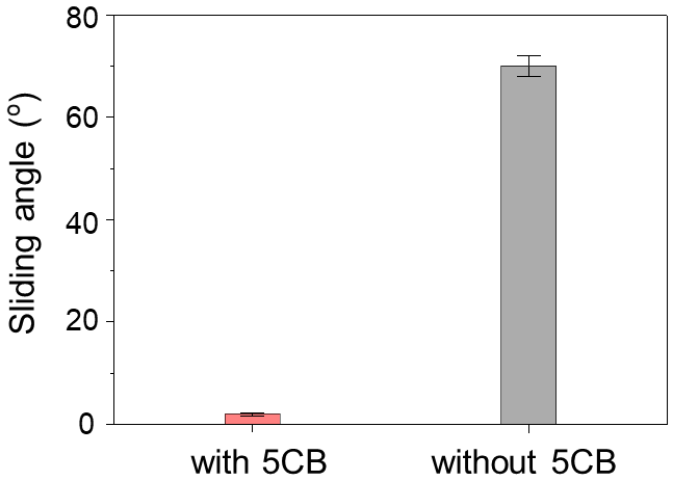

Figure S9. Sliding angle of water droplets on a polyRM257 structure (red) filled with 5CB with excess 5CB on the surface and (gray) without any 5CB on the surface or in the structure. The droplet volume was 2 µL.

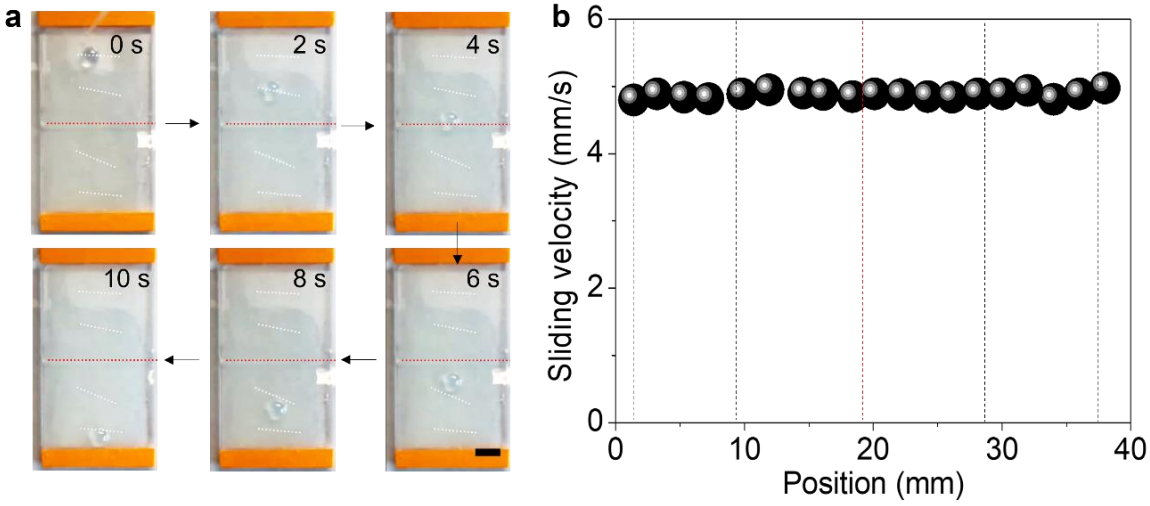

Figure S10. Physical stability of LC-based open surfaces. a) Time-lapse photographs showing the pinning-free sliding of water droplets on two connected nematic 5CB surfaces after being physically damaged. The tilting angle of the LC surface was 30º and the water droplet volume was 10 µL. Scale bar, 5 mm. b) Plot showing the sliding velocity of water droplets on the 5CB surface. Black and red dashed lines indicate the location of the razor cuts and the junction between the two LC surfaces, respectively.

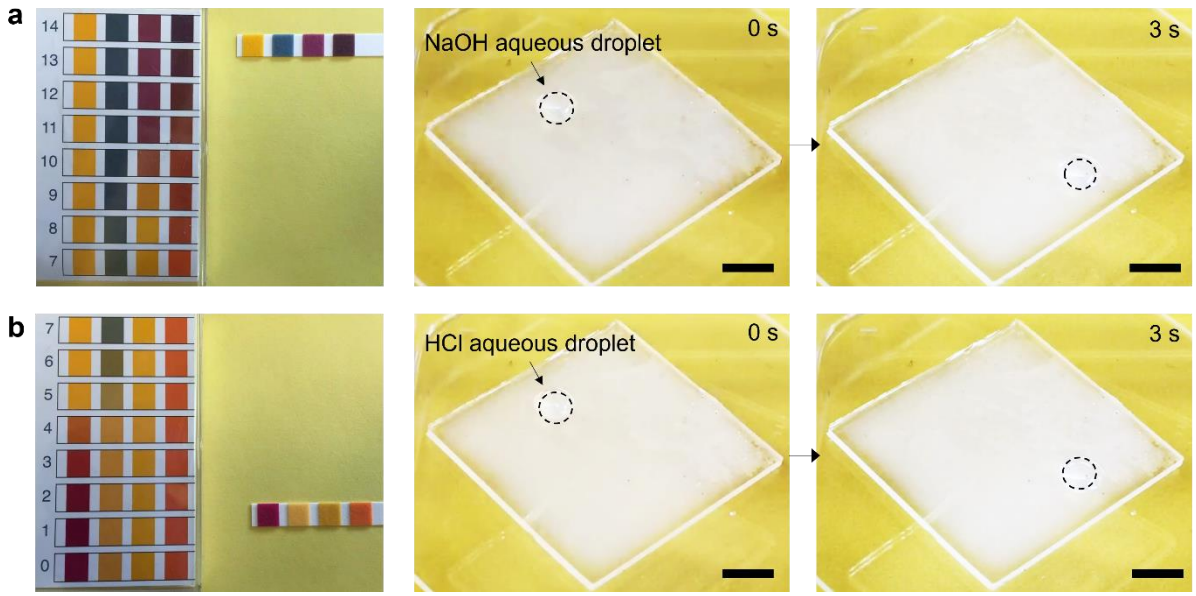

Figure S11. Water droplets with different pH values on the LC-based open surfaces. a,b) Photographs showing both NaOH (pH = 13) and HCl (pH = 1) aqueous droplets can slide without pinning on the nematic 5CB surface. The pH value does not affect the sliding angle of the water droplets on the 5CB surfaces. The water droplet volume was 10 μL and the substrates were tilted at 7°. Scale bars, 0.5 cm.

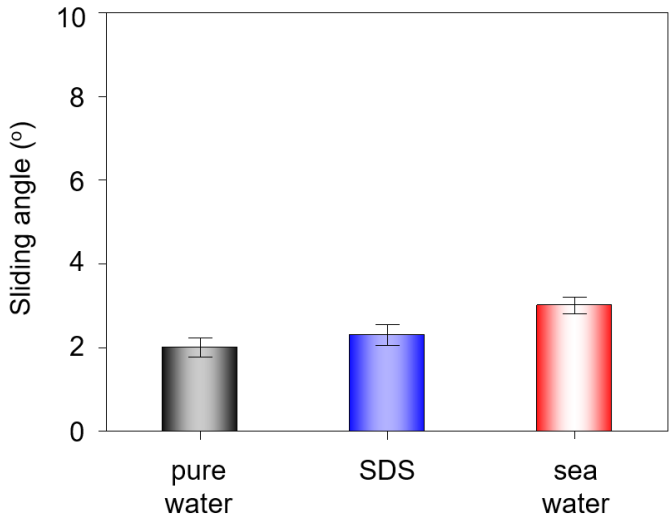

Figure S12. Effect of SDS and artificial sea salt on the sliding angle of water droplets on LC surfaces. The concentration of SDS was 5 mM. The artificial sea water was a mixture of $MgCl_2$ (0.226 g), $MgSO_4$ (0.325g), NaCl (2.673g) and $CaCl_2$ (0.112 g) in 100 mL of deionized water. The volume of each water droplet used in this experiment was 2 μL. Error bars represent standard deviations. n = 3 for each data point.

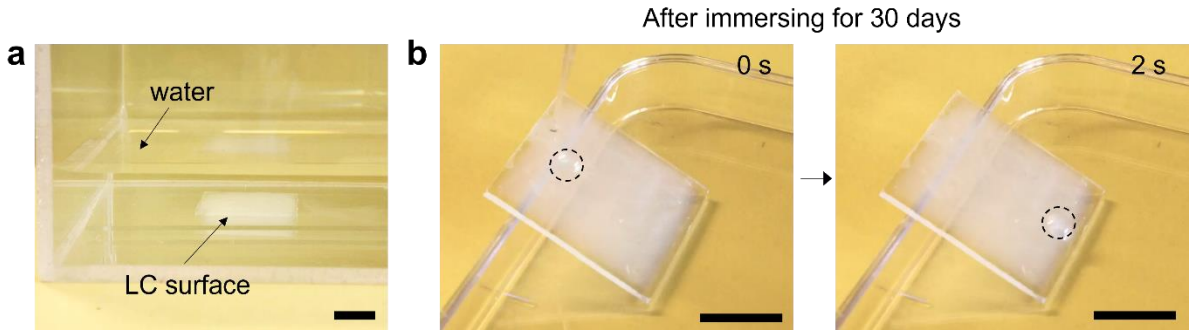

Figure S13. Underwater durability of LC-based open surfaces. a) Photograph showing the LC immersed in water. b) Photographs showing that a water droplet can slide off the nematic 5CB surface after being immersed in water for 30 days. The tilting angle of the LC surface was 10^{o} and the water droplet volume was 10 µL. Scale bars, 1 cm.

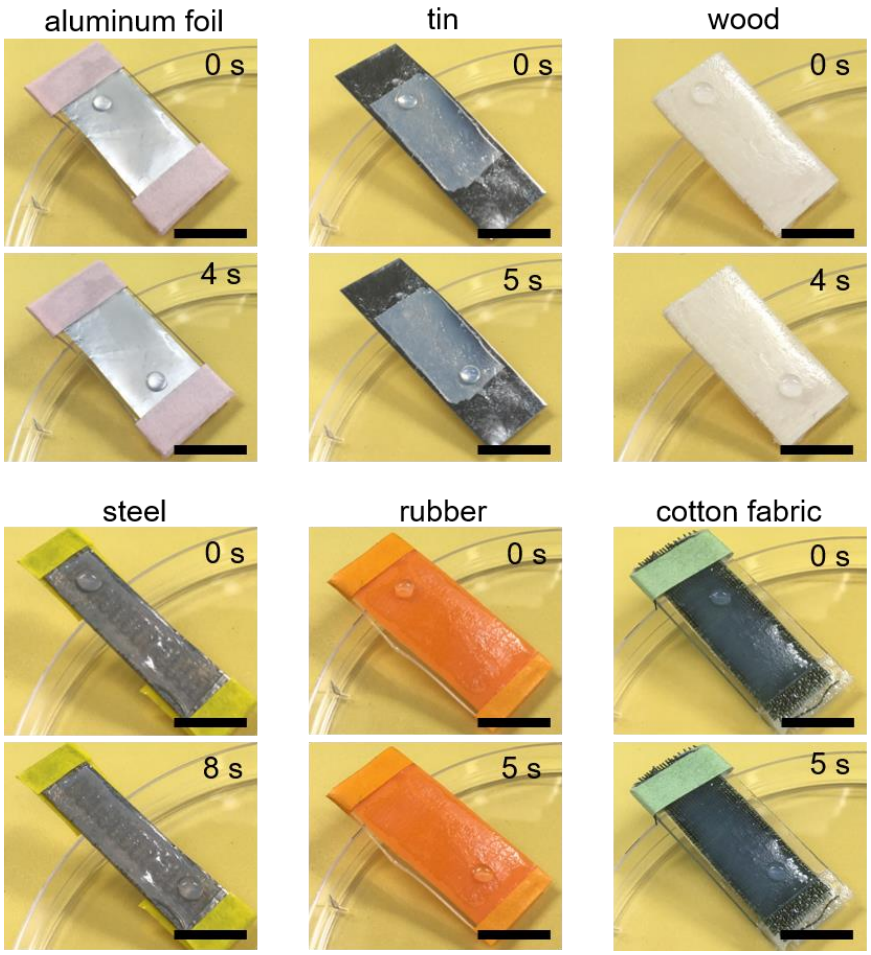

Figure S14. Demonstration of LC coatings on a variety of substrates. Photographs showing the pinning-free sliding of water droplets on 5CB films coated on different substrates. The water droplet volume was 2 μL and the substrates were tilted at 7°. Scale bars, 1 cm.

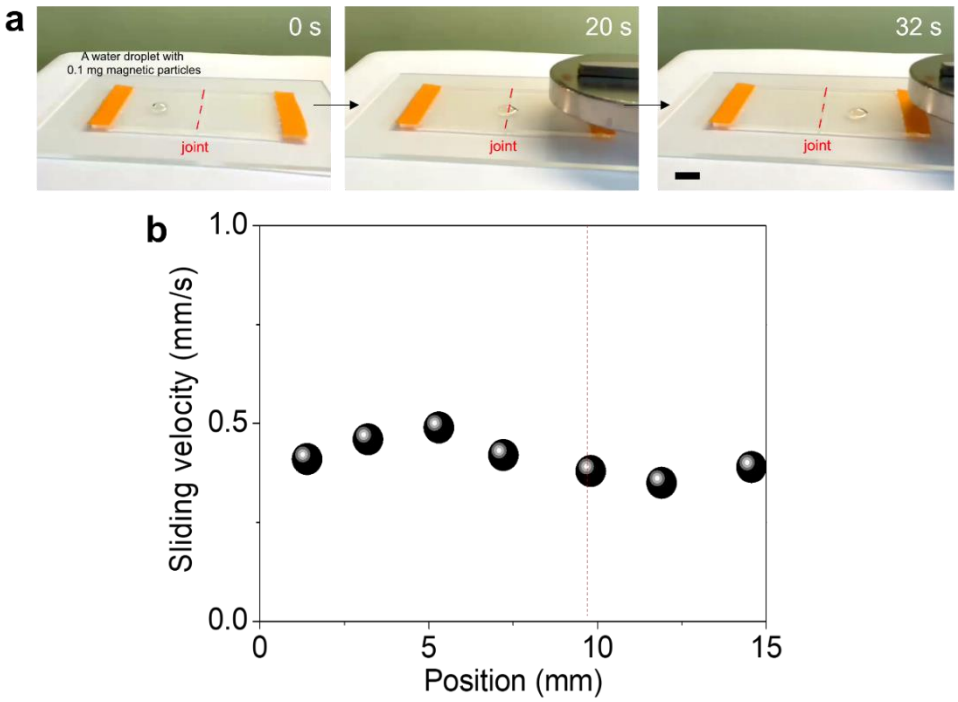

Figure S15. Remote control of water droplets sliding on LC-based open surfaces. a) Time-lapse photographs showing the pinning-free sliding of a water droplet with 0.1 mg of magnetic Fe_3O_4 particles on two connected nematic 5CB surfaces in the presence of an external magnetic field (0.56 T). The water droplet volume was 10 µL. Scale bar, 5 mm. b) Plot showing the sliding velocity of water droplets on the 5CB surface under a magnetic field (0.56 T). The red vertical dashed line indicates the junction between two LC surfaces.

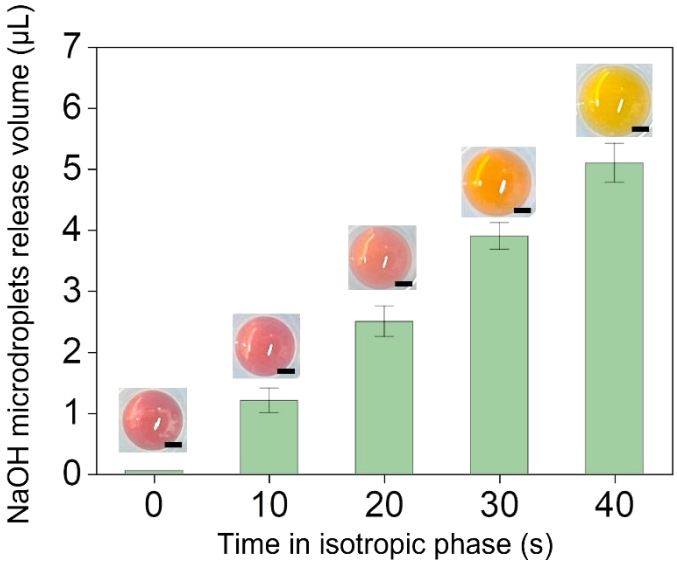

Figure S16. Plot showing the amount of NaOH aqueous microdroplets released from the LC surface to the aqueous droplet on the LC surface as a function of the duration the 5CB film was in the isotropic phase (40°C). Insets show the photographs of the aqeous droplets on the LC surface. The volume of the aqueous droplet on the LC surface was 10 μL and the concentration of the methyl orange was 0.5 mM. Scale bars, 1 mm.

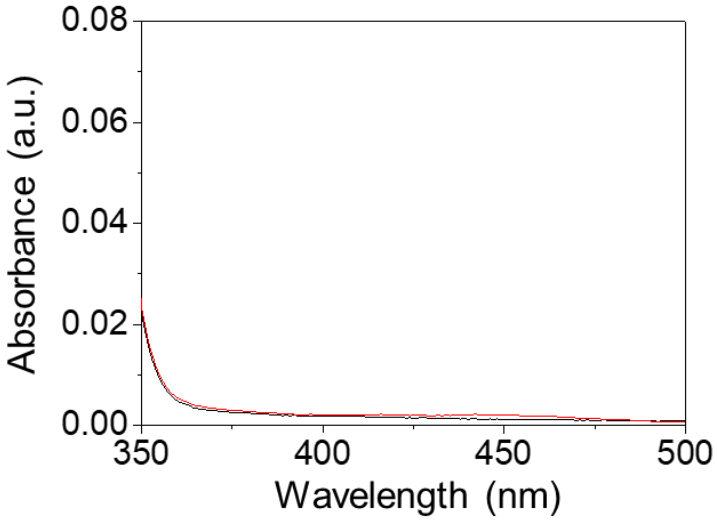

Figure S17. Effect of droplet movement on the transfer of ethyl orange aqueous microdroplets between different LC film modules. UV–visible spectra of (black curve) pure 5CB as a control experiment and (red curve) the 5CB under a water droplet after it was evaporated. This water droplet was moved from a LC film with encapsulated ethyl orange aqueous microdroplets in the nematic phase (25^{o}C) to a pure LC film. The mass of the ethyl orange aqueous microdroplets in the LC film (2.5 cm × 2.5 cm) was approximately 12 mg. The volume of the water droplets was 10 μL.

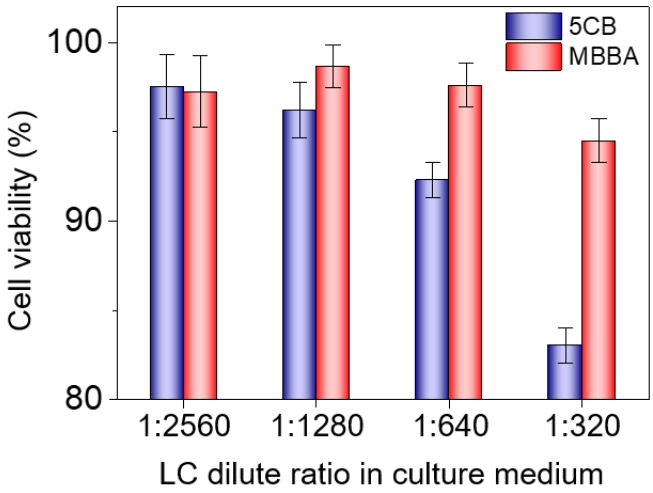

Figure S18. Cytotoxicity analysis of LCs. hiPSCs (1×10^4) in 100 µL of a culture medium were plated in each well of a 96-multiwell plate for overnight growth. After removal from the culture medium, the hiPSCs were treated with different ratios of LC to culture medium for 24 h and the cell viability was measured.

Movies

Movie S1. Chemicals release on the LC-based open surfaces. Three 10 μL water droplets were placed on LC-based open surfaces, which contained nanometer-sized aggregates of ethyl orange in 5CB and aqueous microdroplets of ethyl orange in 5CB and E7, respectively. The nanometer-sized aggregates were immediately released into the water droplet. The aqueous microdroplets were released from the 5CB film following a temperature increase to 40ºC, which triggered a nematic to isotropic phase transition ($T_{N\text{-}I,\ 5CB}$ is approximately 35ºC). Finally, the aqueous microdroplets were released from the E7 film following a temperature increase to 65ºC, which triggered a nematic to isotropic phase transition ($T_{N\text{-}I,\ E7}$ is approximately 62ºC).

Movie S2. Physical stability of LC-based open surfaces. We connected two individual LC surfaces together and made four independent scratches on the LC surfaces using a razor. A 10 μL water droplet was placed on the LC-based open surface. The tilting angle of the LC surface was 30º. The water droplet can be seen to move freely over the scratches in the LC surfaces and the joint between them.

Movie S3. Remote control of water droplets on LC-based open surfaces. Two LC surfaces were connected together to provide a platform for a water droplet to slide across. A 10 μL water droplet with 0.1 mg magnetic particles was placed on the LC surfaces. The water droplet can be seen to move on the LC surfaces after a magnetic field is applied (0.56 T).

Movie S4. Instructions for LC-based chemical feeding device. First, hiPSCs were cultured and placed in opposite ends of our 4-chambered cell differentiating device. Next, a LC platform created with a combination of three different LC modules was installed on the two other chambers. The different colors of the LC modules represent different encapsulated chemicals or growth factors: VEGF (cyan), CHIR (yellow), and Wnt-C59 (pink). We then placed a 30 μL water droplet with magnetc particles on the LC surface. We used local Joule heating to induce a phase transition of the VEGF-encapsulated LC module on demand. Afterwards, the chemical or growth factor-containing water droplet was moved into the hiPSC culture medium by using an electromagnet.

Reference

[1] X. Lian, X. Bao, A. Al-Ahmad, J. Liu, Y. Wu, W. Dong, K. K. Dunn, E. V. Shusta, S. P. Palecek, *Stem Cell Rep* **2014**, *3*, 804.

[2] a) Z. Yang, N. L. Abbott, *Langmuir* **2010**, *26*, 13797; b) U. Manna, D. M. Lynn, *Adv. Mater.* **2015**, *27*, 3007; c) Z. Wang, Q. Xu, L. Wang, L. Heng, L. Jiang, *J. Mater. Chem. A* **2019**, *7*, 18510.

[3] T. S. Wong, S. H. Kang, S. K. Tang, E. J. Smythe, B. D. Hatton, A. Grinthal, J. Aizenberg, *Nature* **2011**, *477*, 443.

[4] M. Kléman, O. D. Lavrentovich, *Soft Matter Physics: An Introduction,* Springer **2003**.

[5] J. N. Israelachvili, *Intermolecular and Surface Forces,* Elsevier **2011**.

[6] C. M. Roth, B. L. Neal, A. M. Lenhoff, *Biophys. J.* **1996**, *70*, 977.

[7] a) O. P. Pishnyak, S. Tang, J. R. Kelly, S. V. Shiyanovskii, O. D. Lavrentovich, *Phys. Rev. Lett.* **2007**, *99*, 127802; b) S. B. Chernyshuk, B. I. Lev, *Phys. Rev. E* **2011**, *84*, 011707; c) T. A. Wood, J. S. Lintuvuori, A. B. Schofield, D. Marenduzzo, W. C. K. Poon, *Science* **2011**, *334*, 79; d) P. Poulin, H. Stark, T. C. Lubensky, D. A. Weitz, *Science* **1997**, *275*, 1770; e) I. Musevic, M. Skarabot, U. Tkalec, M. Ravnik, S. Zumer, *Science* **2006**, *313*, 954.

[8] J. K. Gupta, S. Sivakumar, F. Caruso, N. L. Abbott, *Angew. Chem. Int. Ed.* **2009**, *48*, 1652.

[9] Y. K. Kim, X. Wang, P. Mondkar, E. Bukusoglu, N. L. Abbott, *Nature* **2018**, *557*, 539.

[10] Y. Xu, A. M. Rather, Y. Yao, J.-C. Fang, R. S. Mamtani, R. K. A. Bennett, R. G. Atta, S. Adera, U. Tkalec, X. Wang, *Sci. Adv.* **2021**, *7*, eabi7607.

[11] a) D. Render, T. Samuel, H. King, M. Vig, S. Jeelani, R. J. Babu, V. Rangari, *J. Nanomater.* **2016**, *2016*; b) S. Kirboga, M. Öner, O. Dogan, *Pure Appl. Chem.* **2016**, *88*, 961.